Materials Science and Engineering B 291 (2023) 116363

Contents lists available at ScienceDirect

Materials Science & Engineering B

journal homepage: www.elsevier.com/locate/mseb

Enhanced magnetoelectric effect in Lead-Free piezoelectric $BaZr_{0.2}Ti_{0.8}O_3$ − 0.5 $Ba_{0.7}Ca_{0.3}TiO_3$ and Fe-rich magnetostrictive $Co_{0.8}Fe_{2.2-x}Dy_xO_4$ nanocomposites for energy harvesting applications

Shahaji P. Kharat [a,b], Swati K. Gaikwad [a,b], Bharat G. Baraskar [a], Debabrata Das [c], R.C. Kambale [a], Y.D. Kolekar [a], C.V. Ramana [c,d,*]

[a] Department of Physics, Savitribai Phule Pune University, Pune-411007, Maharashtra, India
[b] Department of Physics, Fergusson College (Autonomous), Pune-411004, Maharashtra, India
[c] Centre for Advanced Materials Research (CMR), University of Texas at El Paso, El Paso, TX 79968, USA
[d] Department of Mechanical Engineering, University of Texas at El Paso, El Paso, TX 79968, USA

ARTICLE INFO

Keywords:
Magentoelectric Composites
Interfacial Effects
Phase-Composition
Piezoelectric Coefficient (d_{33}), Magnetoelectric (M−E) Effect
Dielectric Properties

ABSTRACT

The design, discovery and development of magnetoelectric (ME) composites with enhanced properties and performance opens up further opportunities to explore new scientific aspects and to develop next-generation electromagnetic devices. Nevertheless, the engineered complex ME composites with multi-phase interfacial chemistry have rarely been reported. In this context, in the present work, enhanced magnetoelectric phenomenon reported for the ME-composites made using lead-free ferroelectric phase $BaZr_{0.2}Ti_{0.8}O_3$–$0.5Ba_{0.7}Ca_{0.3}TiO_3$ (BZT-BCT) and magnetostrictive phase $Co_{0.8}Fe_{(2.2-x)}Dy_xO_4$ (CFDO). The ME composites were synthesized by varying the magnetostrictive CFDO phase, where Dy(x) varied as x = 0.000(ME1), 0.025 (ME2), 0.050 (ME3) and 0.075 (ME4). The effect of varying CFDO phase on the structure, morphology, microstructure, density, piezoelectric, dielectric, ferroelectric and magnetoelectric properties of the ME-composites is evaluated. X-ray diffraction analyses of all ME-composites confirm the tetragonal structure of the BZT-BCT ferroelectric phase and spinel cubic structure of the CFDO ferrimagnetic phase. Raman spectroscopic analyses also confirm and validate the respective phases with a clear signature presence of the characteristics modes. Granular, dense microstructure with a uniform particle size distribution evidenced in scanning electron microscopy imaging analyses. The physical density measurements indicate that the ME composites attain a density in the range of 6.0–6.4 g/cm^3; density increases with increasing CFDO phase. Frequency dispersion profiles of the dielectric constant exhibit a maximum dielectric constant for ME1 composite while a sharp decrease in dielectric constant at higher frequencies is noted with increasing CFDO phase in the ME-composites. Ferroelectric properties evaluated by measuring the polarization (P) – electric field (E) hysteresis loops at 300 K indicate the presence of typical P-E loops in all ME composites confirming that the ferroelectric properties are retained even after combining with the magnetic phase. The ME4 composite demonstrate a 0.573 squareness ratio, which is useful for multistate memory device applications. The ME4 composites further characterized by a moderately higher remnant polarization (P_r = 2.24 μC/cm^2). All the synthesized ME-composites are promising for permanent memory storage device (FeRAM) applications. Piezoelectric coefficient measurements indicate a maximum piezoelectric coefficient of 116 pC/N for the ME4 composite while the ME-coefficient measurements demonstrate higher ME-coefficients of 250 mV/(cm-Oe) for ME2 composite. Based on the comprehensive and comparative studies of the ME-composites with variable magnetostrictive phase, the structure-chemistry-property correlation in these ME-composites established for possible applications in electromagnetic devices and energy harvesting applications.

* Corresponding author at: Centre for Advanced Materials Research (CMR), University of Texas at El Paso, El Paso, TX 79968, USA.
E-mail address: rvchintalapalle@utep.edu (C.V. Ramana).

https://doi.org/10.1016/j.mseb.2023.116363
Received 31 October 2022; Received in revised form 6 February 2023; Accepted 8 February 2023
Available online 20 February 2023

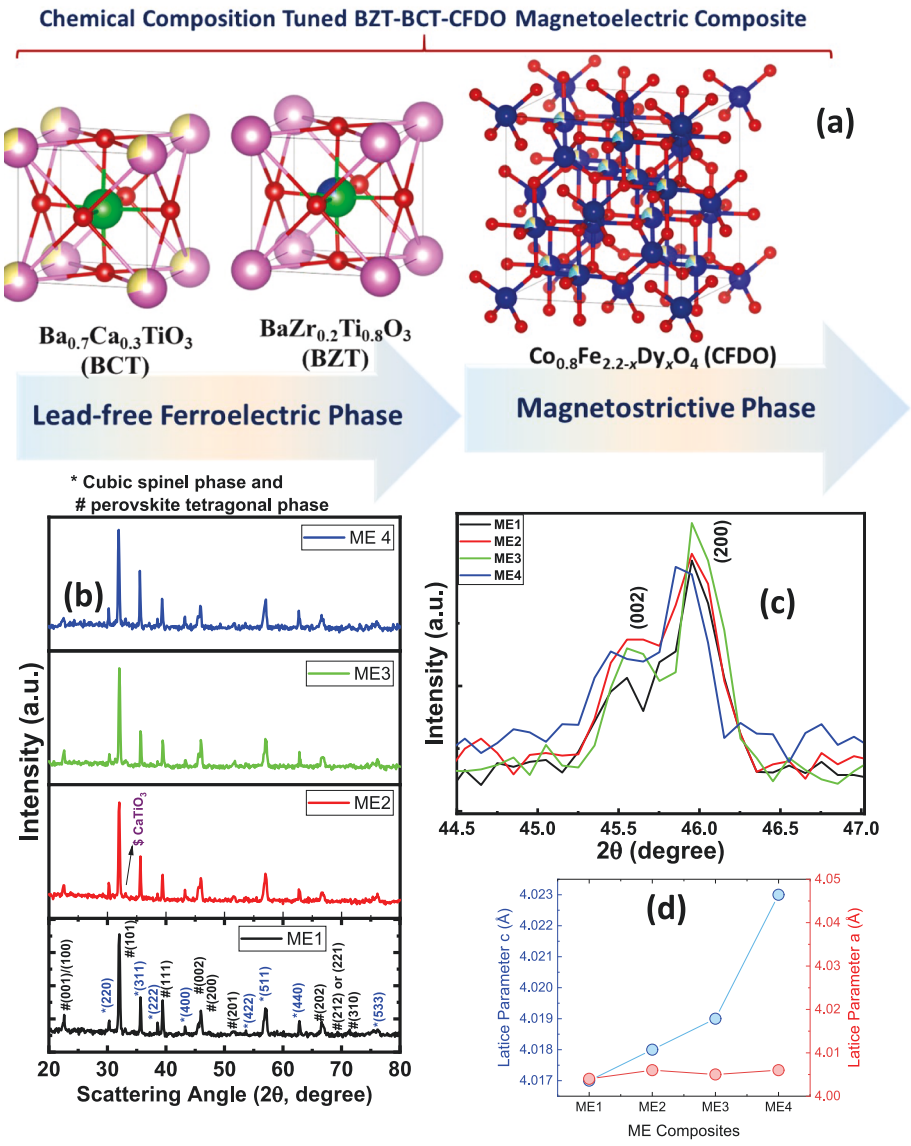

Fig. 1. (a) Schematic representation of the respective phases and the ferroelectric/piezoelectric phase integration with magnetostrictive phase considered to design the ME-composite. (b) X-ray diffraction patterns of all ME composites. The perovskite tetragonal phase is shown by #, cubic spinel phase is shown by * and impurity peak corresponding to $CaTiO_3$ phase is shown by $. The data indicates the presence of ferroelectric and magnetostrictive phases without any chemical/sintering-reaction induced phase degradation. (c) Doublet in XRD of ME composites. The doublet peak confirms the tetragonal structure of the ferroelectric phase in the ME composite. (d) The lattice parameter variation of the tetragonal phase. The lattice expansion in *c*-direction can be noted.

1. Introduction

Magnetoelectric (ME) coupling phenomena, the ME-materials' design and development, and device efficiency tuning are attracting the attention of scientific and engineering community enormously due to their multitude of applications in many technologies[1,2]. The current surge in the ME composite materials is fueled by both the potential technological applications and underlying new fundamental science because of the coupling phenomena. The specific recent trends toward device miniaturization led to an increased scientific interest in combining magnetic and electronic properties into multifunctional materials, so that a single device can perform multiple tasks with a high precision. However, attempts to design ME devices that combines magnetism and ferroelectricity in the same phase have proved unexpectedly difficult[3]. ME composite materials have a higher magnetoelectric voltage coefficient than single-phase magnetoelectric materials [4]. Despite scientific and technological challenges, when engineered taking the fundamental materials' science and engineering aspects or principles into consideration, the appropriate properties of the individual phases invoked in ME-composites so as to realize a composite that can exhibit a sum or product of the properties or even combination of several properties. Thus, the ME effect in composite ME is extrinsic (because neither the piezoelectric nor magnetic phase has the ME effect, but composites of these two phases have remarkable ME effect), depending on the composite microstructure and coupling interaction across magnetic-piezoelectric interfaces[3].

The ME composite materials typically retain the magnetic and ferroelectric properties of their constituent phases. As a result, all the technological requirements/applications of the magnetic and ferroelectric materials are readily fulfilled by ME composites and find numerous applications in electromagnetic devices[1,2,5–7]. Additionally, due to their attractive ME characteristics, either new applications are continually evolving or exploiting ME-composites in different applications in fields other than traditional electromagnetics is explored [1]. The fundamental aspect of ME composite for a given technological application lies in the magneto-electric coupling between two or more ferroic order parameters simultaneously present in the materials[8]. The ferroelectric, ferromagnetic, and ferroelastic orderings are observed between polarization–electric field, magnetization-magnetic field, and stress–strain, respectively[4]. Furthermore, there is a new order that has been coined recently is ferro-toroidic ordering[9]. All these ferroic orders and the fundamental science of interlinking between them stimulates the scientific and research community to envision a variety of device applications in electronics, magnetics and electromagnetic

industries. In fact, the ME composites have opened a new area of research and will allow the development of completely novel devices such as energy harvesters, magnetic field sensors, power efficient antennas, multistate memory devices, voltage tunable inductors, etc [1,2,5–7]. Also, novel ME materials open many opportunities for communication systems, non-volatile memory devices (Me-RAM), spintronics devices, etc[10,11]. Additionally, when these ME-composites are eco-friendly, they are useful for sustainable development. For instance, and the best example to mention is, if Pb-free materials are used in the ME-composites for energy harvesters, they can substantially contribute towards the renewable green source of energy [12].

In connection with the constituent phases of ME composite materials, efforts directed to search for superior Pb-free piezoelectric phase and also to enhance magnetostrictive stress sensing (dλ/dH)[13–15]. In this context, perovskite materials have received a lot of attention from scientists recently because of their diverse structural characteristics and wide range of uses as superconductors, metals, semiconductors, insulators, ferromagnets, antiferromagnets, ferroelectrics, multiferroics, dielectrics, and piezoelectrics, among others[16–20]. The efforts resulted in some novel Pb-free materials; among those, the morphotropic phase boundary[18] composition $BaZr_{0.2}Ti_{0.8}O_3$–0.5 $Ba_{0.7}Ca_{0.3}TiO_3$ (BZT-BCT) reported for superior ferroelectric and piezoelectric properties[16,21]. Similarly, in recent years, extensive efforts undertaken to synthesize magnetostrictive stress sensing materials[13–15,22–24]. It is well known that for designing high-quality actuators and magnetic field sensors, values of the magnetostriction coefficient (λ) and strain sensitivity (dλ/dH) must be higher[13,14]. In this context, cobalt ferrite materials are excellent candidate materials and preferred choice due to its high coercivity and magneto-crystalline anisotropy. Specifically, iron-rich cobalt ferrite, $Co_{0.8}Fe_{2.2}O_4$ has considerably attracted the attention of scientific community due to its large magnetostriction coefficient λ = -590 ppm, measured along the (1 0 0) direction[5,25,26]. Also, the Dy^{3+} substitution for Fe^{3+} in $Co_{0.8}Fe_{2.2}O_4$ showed higher strain sensitivity. Thus, in the present work, $C_{0.8}Fe_{2.2}O_4$ with Dy^{3+} substitution (referred to CFDO hereafter) chosen as a magnetic phase while BZT-BCT is chosen as a ferroelectric phase for the synthesis of ME-composite materials[15]. The goal is to explore the ME effects in this multi-phase system, where the best properties reported for individual component magnetic and ferroelectric phases, to realize materials for energy harvesting applications. The key idea to integrate the ferroelectric and ferrimagnetic phases to design the ME-composite is schematically presented in Fig. 1a. While synthesizing the multi-phase materials with integrated structure, chemistry, interfacial phase-separation and retaining properties without degradation is quite challenging, especially at the nanoscale dimensions, we directed our efforts to synthesize the best quality ME-composites based on the BZT-BCT-CFDO system of materials.

For the synthesis of ME composite materials, a variety of methods are available[1,2,5–7]. However, several challenging scientific problems exists with the synthesis of magnetoelectric composites with desirable phase and property[1,27]. For example, the ferroelectric phase and magnetostrictive phases may chemically react with each other and results into an additional/impurity phase(s)[1,4,28]. Similarly, the processing conditions, especially the sintering temperature strongly influences the chemistry and properties of the resulting ME composites. Typically, when ME composites are sintered at higher temperatures, they lead to the lower value of ME coefficients[1,27]. Such degradation in the properties occurs mostly due to: (i) interdiffusion, (ii) melting point mismatch, and (iii) thermal expansion coefficient mismatch between the ferroelectric and magnetic phases[1,27]. Furthermore, even if these problems are optimized, one of the challenging problems that may continue for ME composites in particulate or thin film or thick film forms is their charge leakage problem that results from the lower resistive ferrite phase compared to the piezoelectric phase[28]. Thus, taking this particular challenging problem into consideration, we directed our attention to CFDO magnetostrictive phase for the ME-composite design due to their higher resistivity compared to other cobalt-based spinel ferrites[4].

Table 1
ME-composites synthesized and the respective component phases in the samples.

S. No.	Ferroelectric Phase Composition (Constant) in ME-Composite	Magnetostrictive Phase Composition (Variable) in ME-Composite	Composite Identification Number
1.	$BaZr_{0.2}Ti_{0.8}O_3$–$0.5Ba_{0.7}Ca_{0.3}TiO_3$	$Co_{0.8}Fe_{(2.2-x)}Dy_xO_4$; $x = 0.000$	ME-1
2.	$BaZr_{0.2}Ti_{0.8}O_3$–$0.5Ba_{0.7}Ca_{0.3}TiO_3$	$Co_{0.8}Fe_{(2.2-x)}Dy_xO_4$; $x = 0.025$	ME-2
3.	$BaZr_{0.2}Ti_{0.8}O_3$–$0.5Ba_{0.7}Ca_{0.3}TiO_3$	$Co_{0.8}Fe_{(2.2-x)}Dy_xO_4$; $x = 0.050$	ME-3
4.	$BaZr_{0.2}Ti_{0.8}O_3$–$0.5Ba_{0.7}Ca_{0.3}TiO_3$	$Co_{0.8}Fe_{(2.2-x)}Dy_xO_4$; $x = 0.075$	ME-4

In the pursuit of better magnetoelectric properties, synthesis of ME composites with different cobalt ferrite based magnetostrictive and barium titanate based ferroelectric phases were carried out by many researchers. The first such effort is reported by Suchetelene in 1972, wherein using the product property, a ME composite with piezoelectric oxide $BaTiO_3$ (BT) and magnetostrictive $CoFe_2O_4$ (CFO) is analyzed[29]. Recently, Abraham et. al. reported ferrite-core ($MgFe_2O_4$) and piezoelectric-shell ($BaTiO_3$) for advanced magneto-electric devices and memories[30]. However, it is difficult to synthesize good core–shell structures with ferrite-core and piezoelectric shells[6]. To improve further, work on microwave-assisted radiant hybrid sintering is also carried out by Upadhyay et. al.[31]. On the other hand, compared to synthesis of thin film composites, synthesis of particulate composite is relatively easy. Also, if one could produce/establish particulate composite with improved ME coefficients then for better results, it may be worth to adopt that for synthesis of thin/thick films. Currently, Pb-based ferroelectric and magnetoelectric materials are dominating the electronics industry because of their superior properties. However, since the restriction on such materials is because of the toxicity of Pb, it is desirable to replace these materials with lead-free materials[32]. Thus, in the present case, we have directed on the ME-composites based on BZT-BCT-CFDO system of materials, measured the magnetoelectric properties, and finally established a structure-chemistry-property correlation for predicting their possible applications. Furthermore, in order to validate ability of these materials in practical applications in energy related technologies, the energy harvesting applications of the BZT-BCT-CFDO-composites are demonstrated.

2. Materials and methods

2.1. Composites synthesis

For the synthesis of magnetoelectric (ME) composites, pure magnetic ($Co_{0.8}Fe_{(2.2-x)}Dy_xO_4$, with × = 0.00, 0.025, 0.050 and 0.075) and piezoelectric ($BaZr_{0.2}Ti_{0.8}TiO_3$-$0.5Ba_{0.7}Ca_{0.3}TiO_3$) phases were synthesized separately. The magnetostrictive $Co_{0.8}Fe_{(2.2-x)}Dy_xO_4$, with x = 0.00,0.025,0.050 and 0.075 were synthesized by using sol–gel auto-combustion method. The detailed procedure for the synthesis is reported in our earlier research paper[15]. Thereafter, ferroelectric BZT-BCT phase was synthesized by using the standard ceramic method. For the synthesis of magnetoelectric composites of BZT-BCT (as a piezoelectric phase) with four magnetostrictive phases ($Co_{0.8}Fe_{(2.2-x)}Dy_xO_4$; x = 0.000, 0.025, 0.050 and 0.075 Dy^{3+} concentrations) were taken and designated as ME1, ME2, ME3, and ME4 respectively. The sample details are included in Table 1. For the ME synthesis, ferroelectric and magnetostrictive samples were taken in 90:10 by weight percent proportion. The chemical reaction of the synthesis is as shown below:

$$10\ wt\%\ \text{of}\ (CFDO) : 90\ wt\%\text{of}\ \ (BZT - 0.5BCT) \rightarrow ME\ \ composite \qquad (1)$$

Table 2
Physical and structural characteristics of the ME composites determined from XRD, SEM, and density measurements.

Code	Lattice parameter (Å)		c/a ratio	Lattice parameter of spinel phase	Density (Archimedes principle) g/cm^3	Average crystallite size (nm)	Average grain size (μm)
	c	a					
ME1	4.017	4.004	1.0032	8.355	6.02	26.24	1.08 μm
ME2	4.018	4.006	1.0032	8.371	6.65	30.49	0.85 μm
ME3	4.019	4.005	1.0032	8.372	6.13	28.83	0.89 μm
ME4	4.023	4.006	1.0042	8.372	6.40	33.21	0.80 μm

Firstly, accurately weighed powders of magnetic and ferroelectric phases were mixed using agate mortar for 5 h. After that binder with 5 wt% polyvinyl alcohol is added in the grinded powder. Then all the magnetoelectric samples were cylindrically pelletized (1 cm in diameter and 1 mm in thickness) using 5 tone/(inch)^2 pressure. These pellets were sintered at 1000 °C for 5 h in an Alumina crucible with a heating and cooling rate of 2 °C/minute.

2.2. Characterization

The structural and phase analyses were carried out using X-ray diffraction (XRD) measurement, which were made using Bruker company (D8 Advance X-ray diffractometer with Cu Kα radiation, λ = 1.5406 Å). The average crystallite size was obtained from the XRD data using the standard method i.e., Scherrer equation[33,34]:

$$D = 0.9\lambda/\beta\cos\theta \quad (2)$$

where D, λ, B, and θ are crystallite size, wavelength of the X-ray, full width half maximum and angle of diffraction peak, respectively. Some of the pellet samples were platinum coated for microstructural analysis using JEOL SEM. To remove the problem of space charge effect arising during secondary electron detection, all the samples were grounded using conducting carbon tape. Also, the atomic and weight percentage measurements were made using energy dispersive spectroscopy (EDS).

The Raman spectroscopic studies were carried out at room temperature using a Renishaw Invia Raman spectroscopy system LEICA DM 2500 M with a 532 nm green light Ar-ion LASER source for the Raman active modes. The Raman scattering peaks were fitted using standard procedures as widely reported in the literature[35,36] in order to obtain reliable and accurate information on the chemical bonding of ME-nanocomposites. The Raman spectra were fitted using the Lorentzian function:

$$I(\omega) = I_0 + \frac{2A}{\pi}\left(\frac{W}{W + 4(\omega - \omega_0)^2}\right) \quad (3)$$

where ω is the phonon frequency of the peak, 'ω_0' is the maximum phonon frequency of the peak, W is full width at half maxima (FWHM), 'A' is the normalization constant, and 'I_0' is the intensity of the background.

For electrical measurements, ME-composite pellets were employed for measurements. The sintered cylindrical pellets with a diameter of 1 cm and a thickness of 1 mm were polished using sandpaper and silver (Ag), which has temperature stability and reasonably good for electrical contacts [37], paste was applied on both the surfaces of pellets for good

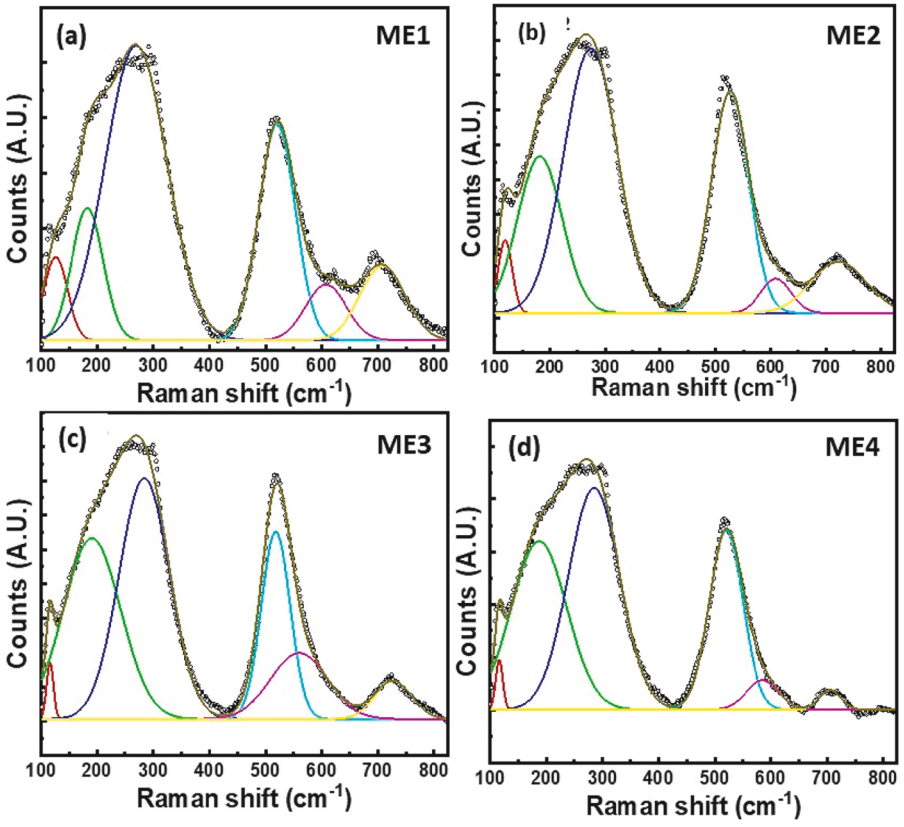

Fig. 2. Raman spectra of the ME composites. The presence of characteristic peaks due to respective phases is evident in Raman spectra. The Raman scattering peaks noted are tabulated in Table 2 along with their assignments. The shift noted in the Raman peaks indicate the sintering-induced strain in ME composites.

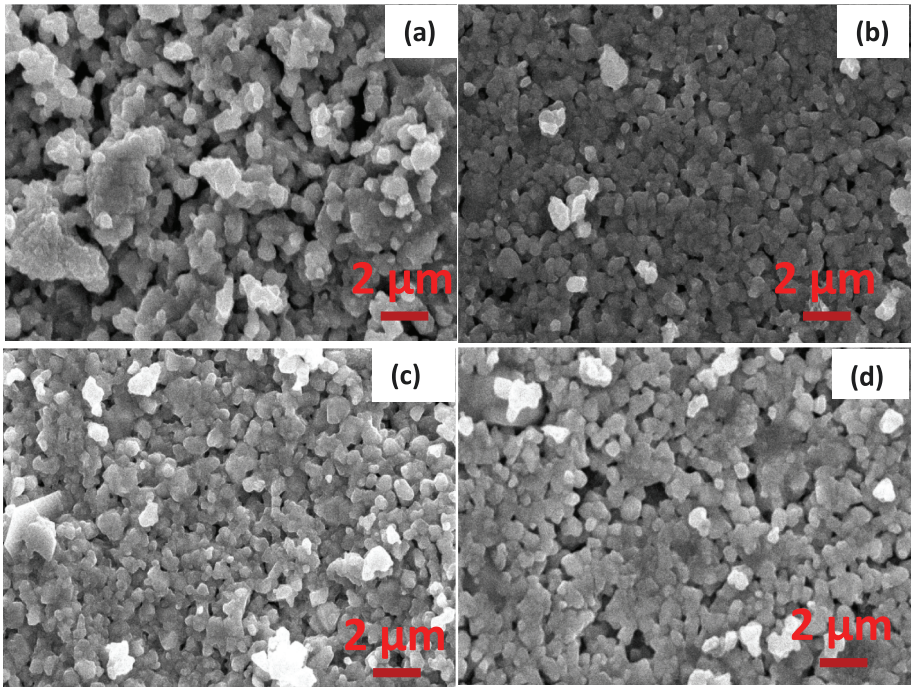

Fig. 3. SEM images of ME composites. The data shown are for: (a) ME1, (b) ME2, (c) ME3, and (d) ME4 magnetoelectric composites.

electrical contacts. Then these pellets were used for dielectric measurements, which were made using a Hioki 3532–50 LCR meter in the range of 42 Hz to 5 MHz. Polarization versus electric field measurements (P vs E hysteresis loops) were performed using a P-E hysteresis loop tracer. Density measurements of all the samples were carried out using Archimedes' principle with toluene solution. The Ag-pasted pellets were electrically poled at an electric field approximately-three times to a coercive field ($E_{poling} = 3E_c$) for 30 min[38]. Silicon oil is used for avoiding the short circuit during dc poling. After aging for 24 h, the electrically poled samples were used to determine the piezoelectric coefficients (d_{33}) using Piezo-d_{33} meter with 250 mN force. Also, the magnetoelectric measurements for all the ME samples were carried after 24 h of poling.

3. Results and discussion

3.1. Structure, phase and chemical bonding

3.1.1. X-ray Diffraction. The X-ray diffraction (XRD) patterns for ME composites are shown in Fig. 1 along with the key idea of the ME-composite design. The XRD patterns (Fig. 1b) indicate the presence of two phases i.e., magnetostrictive spinel phase with space group Fd $\overline{3}$ m and ferroelectric tetragonal phase with *P4mm* space group[15,32]. The peaks indexed in blue color and with a * symbol represent the diffraction from the crystal planes of CFDO phase while black color with a symbol # represent those from BZT-0.5BCT ferroelectric phase. Formation of a minor or small amount of $CaTiO_3$ phase (represented by $) is evident. This is due to the solubility limit ($x = 0.23$) of Ca^{2+} substitution for Ba^{2+} in $Ba_{1-x}Ca_xTiO_3$ phase[39]. No evidence of chemical reaction between the magnetic and ferroelectric phase is seen from any pronounced impurity peak in any of the ME composites. This is made possible by means of the careful optimization of sintering temperature for the constituent phases along with their ME composites. However, the ME composites are heated above 1000 °C, then samples may melt with chemical reaction between the respective phase. Similarly, if it is heated below this temperature, the composite sample will not be sintered properly to transfer the strain between magnetostrictive and ferroelectric phases. The XRD patterns for all ME samples show doublet, which is located at around 2θ = 45.5°, which represents the tetragonal nature of all the ME composites (Fig. 1c). The first peak corresponds to (002) and the second peak corresponds to (200) planes. The presence of doublet i.e., tetragonality confirms the ferroelectric nature of the ME samples. Furthermore, it can be seen (Fig. 1d) that, there is a tetragonal lattice expansion (*c*-direction) varying composition from ME1 to ME4. Table 2 summarizes the structural parameters, density, crystallite size, and grain size for all the ME composites. The X-ray diffraction pattern shows that the average crystallite size, calculated using Scherrer formula, varies from 26.2 nm to 33.2 nm for all the synthesized ME samples.

3.1.2. Raman Spectroscopy.

Spectroscopic characterization, especially using Raman scattering, proved to be quite useful to ascertain the chemical bonding and structural quality of composite materials. Note that Raman spectroscopic analyses provide direct, accurate information on the chemical bonding, especially under the influence of dopants and/or interfacial chemical adsorbates[40,41]. Therefore, we relied on detailed Raman spectroscopic measurements to understand the effect of respective phases fused in the resulting ME-composite. Fig. 2 present the Raman spectra of ME composites. Corroborating with XRD data, Raman spectra also indicate the presence of Raman-active modes corresponding to both ferroelectric and magnetostrictive phases in ME composites. Raman active modes observed for all the ME samples are tabulated in Table 3. The $T_{1g}(3)$ and $A_{1g}(2)$ modes exhibit higher intensity Raman active modes in pure magnetostrictive phases. Whereas, other modes (A1 (TO2), A1 (TO3) and A1 (LO3)) correspond to ferroelectric BZT-BCT phase. The shift in the Raman active modes corresponds to the strain generated in the sintering of ME composite samples.

3.2. Morphology, microstructure and density

The SEM images of ME composites shown in Fig. 3 reveal uniform grains, where the grain boundaries are also visible. The SEM micrographs indicate the variation in morphology and microstructure of the ME composites. The average grain size varies in the range of 0.8 μm to 1 μm (Table 2). It is well known that microstructure and grain size along with size-dispersion and/or size-variation tailor the piezoelectric

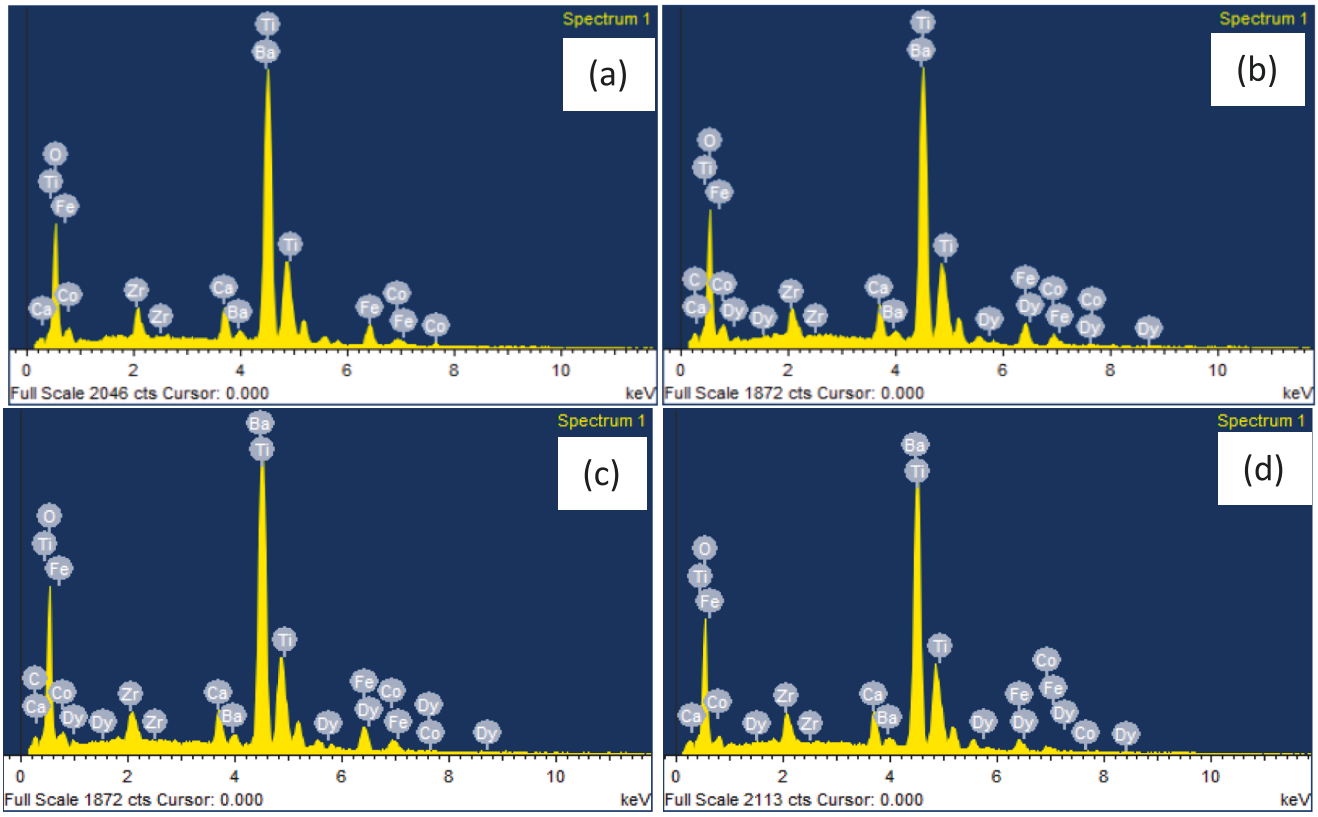

Fig. 4. The EDS spectra of: (a) ME1, (b) ME2, (c) ME3, and (d) ME4 magnetoelectric composites. The spectra indicate the X-ray peaks due to respective elements present in the ME-composites. The composition is summarized in Table 3.

Table 3
Raman modes and peak positions of the ME composites.

Modes	Ref. Raman mode (cm^{-1})	Observed Raman mode (cm^{-1})			
		ME1	ME2	ME2	ME3
[42]$E_{2g}(1)$	–	125.81	119.04	115.61	116.25
[43]$T_{1g}(3)$	204	182.67	181.64	190.78	187.02
[43]A1 (TO2)	259	269.35	273.8	283.98	284.67
[43]A1 (TO3)	521	520.59	526.36	518.11	520.03
[43]$A_{1g}(2)$	613	607.43	609.57	559.58	584.69
[44]A1 (LO3)	715	708.43	722.96	727.31	705.11

properties of ceramics[45,46]. The density measurements were carried out to understand the physical properties in correlation with microstructure; the results are tabulated in Table 2. As expected from the SEM images, the density of ME1 is 6.02 g/cm^3 which is minimum with maximum pores and the density of the ME2 sample is 6.65 g/cm^3 which is maximum with minimum pores on the surface.

Fig. 4 shows the energy dispersive spectra (EDS) of ME composites. Though the composite is a complex sample, the X-ray energy is characteristic of specific atom involved in the X-ray generation [36,37]. Therefore, detection of X-rays emitted provides the signature of the atoms present in the composite samples. As such, EDS measurements and mapping analyses can be used to qualitatively discuss the chemical quality and chemical homogeneity of ME composites[47,48]. The presence of all the elements is confirmed by EDS spectra. The elemental composition (Table 4) also confirms the chemical homogeneity of all the synthesized magneto-electric composites.

3.3. Dielectric and ferroelectric properties

Fig. 5 shows the dielectric and ferroelectric properties measured for ME composites. Fig. 5a shows the frequency response of the dielectric constant of all ME composites. The dielectric constant values for all the

Table 4
Elemental composition of all magneto-electric samples as determined from EDS.

Sample	ME1		ME2		ME3		ME4	
Element	wt%	at%	wt%	at%	wt%	at%	wt%	at%
C K	0	0	3.77	9.56	5.27	12.84	0	0
O K	36.11	75.89	36.79	69.98	37.30	68.25	37.70	77.38
Ca K	1.90	1.60	1.81	1.38	1.72	1.25	2.09	1.71
Ti K	11.2	7.86	10.18	6.47	9.79	5.99	11.18	7.66
Fe K	3.54	2.13	3.18	1.73	3.48	1.82	1.84	1.08
Co K	1.37	0.78	2.19	1.13	1.84	0.91	1.24	0.69
Zr L	4.04	1.49	3.66	1.22	2.62	0.84	4.05	1.46
Ba L	41.83	10.24	38.83	8.60	37.95	8.09	41.63	9.96
Dy L	0	0	0.01	0.01	0.03	0.01	0.27	0.05

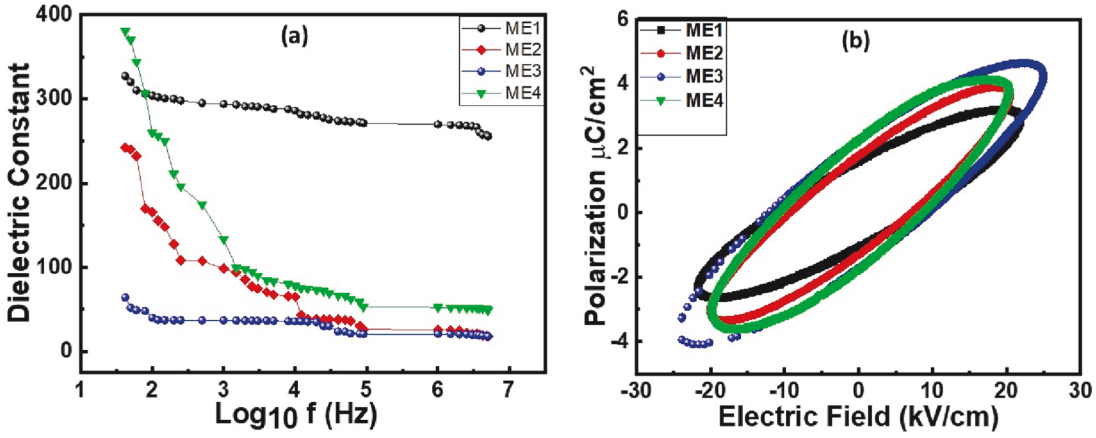

Fig. 5. (a) The frequency response of the dielectric constant of ME composites. (b) P-E hysteresis loops for ME composites.

Table 5
The dielectric constant of the ME composites.

Composition	Maximum value of dielectric constant (at 42 Hz)	Dielectric constant at high frequency (at 5 MHz)	% drop in ε'
ME1	327	271	17.1
ME2	242	26	89.2
ME3	61	19	68.8
ME4	383	55	85.6

Table 6
Ferroelectric parameters determined from PE loops for ME composites.

Composition	P_{max} μC/cm^2	P_r (μC/cm^2)	E_c (KV/cm)	E_{max} (KV/cm)	Squareness ratio
ME1	3.17	1.60	7.86	21.8	0.505
ME2	3.89	1.76	6.89	20.4	0.452
ME3	4.66	2.25	9.19	24.9	0.483
ME4	3.91	2.24	8.60	20.2	0.573

samples are presented in Table 5. It is seen that the ME1 sample has the highest value 271 of dielectric constant at high frequency (5 MHz). Among all the samples, the minimum drop (~17 %) in the dielectric constant is observed for the ME1. A sharp decrease in dielectric constant is attributed to leakage of current due to lower resistance of the ferrimagnetic phase[49]. An apparent evidence of Dy^{3+} substitution is seen as a sharp decrease in the dielectric constant with increasing frequency. Since dielectric constant is a measure of the amount of charge that the material can hold after the application of the electric field, we expect that the ME1 sample (compared to other ME2, ME3, and ME4 composites) may be suitable for ferroelectric capacitor applications. As expected, the dielectric constant (ε') of the ME composite materials decreases rapidly with increasing frequency (from 42 Hz to 5 MHz) and then reaches a constant value (see, Table 5). Thus, the trend seen in dielectric constant and P-E loops can be accounted for the respective phases and microstructure of the ME composites.

Furthermore, as the frequency increases, the ionic and orientation polarizabilities decrease, and finally contribution due to ionic and orientation polarizabilities become negligible due to the inertia of molecules and ions in ME materials. A maximum drop (85.6 %) in the dielectric constant was observed for ME4 composite. The large values of (ε') at lower frequencies for all the composites may be due to heterogeneity, which gives rise to interfacial polarization. The dielectric constant of all the composites can be explained based on Koop's two-layer model (layers of less resistive magnetic and higher resistive ferroelectric materials) and Maxwell-Wagner polarization theory[50]. Since the space charge carriers in the inhomogeneous dielectric structure described requires sufficient time to align the axis parallel to an alternating electric field, therefore there is a decrease of dielectric constant with increasing frequency. Moreover, in the ferrite phase, a sharp fall of resistance is observed and this may be due to the exchange of electrons between Fe^{2+} to Fe^{3+} ions[51].

Fig. 5b shows the room temperature polarization–electric field i.e., P-E hysteresis loops for ME composites. With an applied electric field, the ferroelectric domain changes the orientation of the polarization direction along the external electric field to minimize the energy[52]. The ferroelectric parameters of ME composites are calculated from P-E hysteresis loops and tabulated in Table 6. Among all the composites, ME4 gives higher remnant polarization (P_r = 2.27 μC/cm^2). ME2 has lower coercive electric field (E_c = 6.89 kV/cm), and maximum value of polarization (P_{max} = 4.66 μC/cm^2) for ME3 sample. Thus, each ME sample has one important peculiar value. Lower E_c values reveal lower energy barriers are needed for polarization rotation which effectively improves the piezoelectric properties. The lower value of piezoelectric coefficients may be due to the leakage charge due to the lower resistance of the magnetostrictive phase[49]. Also, the non-uniform grain sized microstructure observed for all ME samples may be essential for higher piezoelectric coefficient.

Table 7
Piezoelectric coefficient values for ME samples.

Composition	d_{33} (pC/N)	Poling electric field (kV/cm)	Dielectric constant
ME1	80	11.20	269
ME2	28	5.62	52
ME3	40	10.07	27
ME4	116	13.20	21

3.4. *Piezoelectric and magnetoelectric (ME) properties*

The piezoelectric coefficient (d_{33}) values of all ME composites are presented in Table 7. It is evident that, the ME4 composite exhibits higher piezoelectric coefficient. While the piezoelectric coefficient is in the range of 28–116 pC/N, the effect of CFDO phase and increasing Dy^{3+} content on the piezoelectric coefficient of the ME-composite is evident. Generally, the piezoelectric properties of the ME composites are strongly affected by three fundamental characteristics, which could result in decreased piezoelectric constant values. The possible chemical reactions that might occur between the piezoelectric and magnetostrictive phases during sintering is the first. Second, the resistivity of magnetostrictive constituent phase may be lower and if the resistivity of magnetostrictive phase is low, complete electric poling is not possible due to leakage of

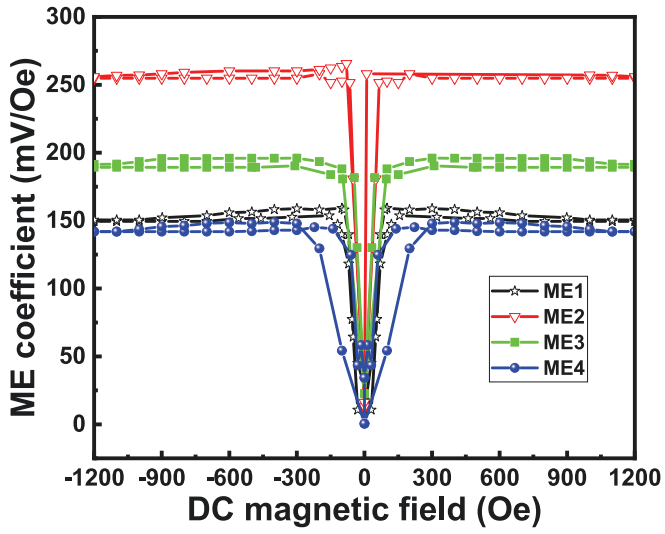

Fig. 6. Magnetoelectric coefficient versus applied dc magnetic field for ME composites.

charge. Also, the leaked charges decrease the magnetoelectric voltage coefficients. Third, mechanical defects such as pores in the sintered ceramics may decrease the piezoelectric coefficient in ME composites. If piezoelectric properties are not good then this leads to the suppression of ME properties. In the present case, the XRD and Raman studies clearly indicate the presence of piezoelectric and magnetostrictive phases well maintained with a phase-interface integrated in the ME-composite. Therefore, the lower value of piezoelectric coefficient for those ME composites with lower Dy content may be due to effect of microstructure, which is characterized by the porous structure of ME composites as seen from SEM images[53].

Note that higher value of magnetoelectric coefficients for ME composites is required for weak magnetic field sensor applications. Our goal is to realize high quality ME composites and to optimize conditions for the purpose. Therefore, in this context, we performed detailed magnetoelectric measurements on the ME composites. Fig. 6 shows the magnetoelectric voltage coefficient with the applied dc magnetic field at ac frequency of 100 Hz. The magnetoelectric voltage coefficient for the ME2 sample is observed to be maximum and it is 250 mV/(cm-Oe). Zhang et.al reported the magnetoelectric coefficient of 150 mV/(cm-Oe) for barium titanate ($BaTiO_3$, BT) layer and an interfacial agent polydopamine (PDA) as the shells are coated on the cobalt ferrite ($CoFe_2O_4$, CFO) nanoparticles[54]. Thus, in the present study, the observed higher value (for the ME2 sample) of magnetoelectric voltage coefficient may be attributed to higher strain sensitivity ($\frac{d\lambda}{dH} = -1.432nA/m$) of the magnetostrictive $C_{0.8}Fe_{2.175}Dy_{0.025}O_4$ phase reported previously[15]. For comparison and to understand the significance of the present approach and elevated nature of the set of ME nanocomposites, the magnetoelectric coefficients of ME nanocomposites in the work are presented and compared with those for other materials reported in the literature in Table 8. It is evident (Table 8) that the ME composites considered in the present study exhibits exceedingly higher values of the magnetoelectric coefficients.

3.5. Energy harvesting applications

Finally, after having understood the structure, physical, chemical, dielectric, ferroelectric, and magnetoelectric properties, we directed our efforts to validate their potential applications in energy harvesting. Specifically, in order to check the ME voltage generated with time varying DC magnetic fields, the ME composites were connected to cathode ray oscilloscope (CRO) and moved the permanent magnet closer and away from the sample to change magnetic flux, which is a measure of their ability for practical applications. The magnetic field of the permanent magnet was 10 Oe. Fig. 7 shows the voltage produced due to time varying magnetic field. Results indicate that the ME composite produces the magnetic field with changing the magnetic flux, which is

Table 8
Magnetoelectric coefficients reported in the literature and ME values obtained for the synthesized samples.

Reference	Compound Name	Magnetoelectric Coefficient mV/(cm.Oe)	Type of materials
This work	$0.10Co_{0.8}Fe_{2.2}O_4$:0.90($BaZr_{0.2}Ti_{0.8}O_3$-0.5$Ba_{0.7}Ca_{0.3}TiO_3$)	159.10	Composite
This work	$0.10Co_{0.8}Fe_{2.175}Dy_{0.025}O_4$:0.90($BaZr_{0.2}Ti_{0.8}O_3-0.5Ba_{0.7}Ca_{0.3}TiO_3$)	250.00	Composite
This work	$0.10Co_{0.8}Fe_{2.150}Dy_{0.050}O_4$:0.90($BaZr_{0.2}Ti_{0.8}O_3-0.5Ba_{0.7}Ca_{0.3}TiO_3$)	196.30	Composite
This work	$0.10Co_{0.8}Fe_{2.125}Dy_{0.075}O_4$:0.90($BaZr_{0.2}Ti_{0.8}O_3-0.5Ba_{0.7}Ca_{0.3}TiO_3$)	147.10	Composite
[55]	CFO@BT@PDA/P(VDF-TrFE)Where ($BaTiO_3$, BT), polydopamine (PDA) ($CoFe_2O_4$, CFO) and poly(vinylidene fluoride-trifluoro ethylene) (P(VDF-TrFE))		Core-Shell
[56]	0.75$CoFe_2O_4$(CFO):0.25$BaTiO_3$(BTO)	5.70	Particulate composite
[56]	0.50CFO:0.50BTO	25.85	Particulate composite
[56]	0.25CFO:0.75BTO	26.90	Particulate composite
[57]	[0.94($Na_{0.5}Bi_{0.5}$)TiO_3–0.06 $BaTiO_3$]:($Co_{0.6}Zn_{0.4}$)-($Fe_{1.7}Mn_{0.3}$)O_4	8.20	Particulate composite
[58]	$Ni_{0.93}Co_{0.02}Mn_{0.05}$- $Fe_{1.95}O_4$ (NMF):$Na_{0.5}Bi_{0.5}TiO_3$ (NBT)	0.155	Particulate composite
[59]	20 %$CoFe_2O_4$:80 %$BaTiO_3$	4.30	Core-shell structure
[59]	25 %$CoFe_2O_4$:75 %$BaTiO_3$	1.83	Core-shell structure
[60]	0.15$CoGa_{0:15}Fe_{1:85}O_4$:0.85$Ba_{0.9}Ca_{0.1}Ti_{0.9}Zr_{0.1}O_3$	52.00	Thin Bilayers
[60]	0.25$CoGa_{0.15}Fe_{1.85}O_4$:0.75$Ba_{0:9}Ca_{0:1}Ti_{0:9}Zr_{0.1}O_3$	82.00	Thin bilayers
[61]	$BaTiO_3$:$CoFe_2O_4$	13.30	Composite fiber
[62]	$BaTiO_3$–$CoFe_2O_4$ (carbon combustion)	0.14	Composite
[63]	Strontium lanthanum doped lead zirconate titanate (PSLZT) - $CoFe_{1.98}Ho_{0.02}O_4$	26.66	Bilayer composite
[63]	PSLZT:$_{0.02}CoFe_{1.97}Ho_{0.03}O_4$	26.66	Bilayer composite
[64]	25 %$BaTiO_3$–75 %$CoFe_2O_4$	1.97	Thin film
[64]	50 %$BaTiO_3$–50 %$CoFe_2O_4$	1.67	Thin film
[64]	75 %$BaTiO_3$–25 %$CoFe_2O_4$	1.23	Thin film

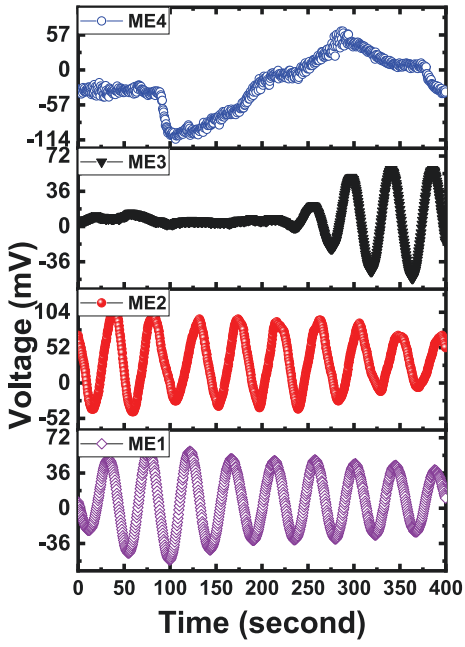

Fig. 7. Magnetoelectric voltage generated with time varying permanent magnet for ME composites.

useful for energy harvesting applications. ME1 and ME2 samples shows variation of the magnetic field with respect to time when permanent magnet is moved closer and away. The ME voltage in ME1 and ME2 samples under investigation shows more than an order of magnitude enhancement in signal compared reference to reported values of the composites which may be due to improved interfacial coupling between two phases[63]. As ME coefficient depends upon the maximum magnetostriction coefficient (λ) of magnetostrictive phase, in the present study the magnetostrictive sample with Dy content ($x = 0.50$) shows highest value of magnetostriction coefficient ($\lambda_{11} = 166$)[15], and thus accounts for the highest value of ME voltage (250 mV) by ME2 composites among all other samples. Overall, the data shown in Fig. 7 is encouraging for the of ME composites for potential energy harvesting applications.

4. Conclusions

We demonstrate the properties and performance of lead-free magnetoelectric composites based on 90($BaZr_{0.2}Ti_{0.8}O_3$–0.5$Ba_{0.7}Ca_{0.3}TiO_3$):10 ($Co_{0.8}Fe_{2.2-x}Dy_xO_4$ with x = 0.000, 0.025, 0.050 and 0.075) materials synthesized by solid-state reaction. X-ray diffraction analyses confirm the formation of cubic spinel phase corresponding to the magnetic phase and perovskite tetragonal phase with a doublet of (002) and (200) for the ferroelectric BZT-BCT phase in all the ME composites. Corroborated with CRD, Raman spectroscopy also validate the presence of both the tetragonal and spinel structures as independent constituent phases. The physical properties, specifically the density and microstructure, depend on the chemical composition which in turn influences the properties and applications of these ME composites. Variation of dielectric constant (ε') with frequency reveals that the ME1 composites, which retains dielectric constant even at a higher frequency (5 MHz), promising for ferroelectric capacitor applications. The maximum value of piezoelectric constant ($d_{33} = 116$ pC/N) is realized for the ME4 composite with Dy^{3+} content high ($x = 0.075$) and will be useful for actuator applications. The ME measurements indicate that the ME2 composite exhibits 250 mV/(cm-Oe) magnetoelectric voltage coefficient, which is highest for the ME composites, particularly compared those with Pb-free piezoelectric constituent phase. These ME2 is useful for energy harvesting and lower magnetic field sensor applications.

Declaration of Competing Interest

The authors declare that they have no known competing financial interests or personal relationships that could have appeared to influence the work reported in this paper.

Data availability

Data will be made available on request.

Acknowledgements

The authors are thankful to the Department of Science and Technology (Government of India), New Delhi for providing financial assistance (Ref. SR/FTP/PS-040/2010) to carry out the research work. S. P. Kharat and S. K. Gaikwad acknowledge the financial assistance from University Grant Commission for Basic Scientific Research (UGC-BSR) fellowships. The authors at the University of Texas at El Paso acknowledge, with pleasure, support from the National Science Foundation (NSF) with NSF-PREM grant #DMR-1827745.

References

[1] N.A. Spaldin, R. Ramesh, Advances in magnetoelectric multiferroics, Nat Mater. 18 (2019) 203–212.
[2] S. Manipatruni, D.E. Nikonov, C.C. Lin, T.A. Gosavi, H. Liu, B. Prasad, et al., Scalable energy-efficient magnetoelectric spin-orbit logic, Nature. 565 (2019) 35–42.
[3] N.A. Hill, Why Are There so Few Magnetic Ferroelectrics? J Phys Chem B. 104 (2000) 6694–6709.
[4] M. Fiebig, Revival of the magnetoelectric effect, J Phys D. 38 (2005) R123–R152.
[5] F. Mushtaq, X. Chen, H. Torlakcik, C. Steuer, M. Hoop, E.C. Siringil, et al., Magnetoelectrically Driven Catalytic Degradation of Organics, Adv Mater. 31 (2019) e1901378.
[6] X. Liang, H. Chen, N.X. Sun, Magnetoelectric materials and devices. APL Mater. 9 (2021), 041114.
[7] C.W. Nan, Magnetoelectric effect in composites of piezoelectric and piezomagnetic phases, Phys Rev B. 50 (1994) 6082–6088.
[8] S. Kopyl, R. Surmenev, M. Surmeneva, Y. Fetisov, A. Kholkin, Magnetoelectric effect: principles and applications in biology and medicine- a review, Mater Today Bio. 12 (2021), 100149.
[9] Y.V. Kopaev, Toroidal ordering in crystals. Phys-Usp. 52 (2009) 1111–1125.
[10] S. Shevlin, Multiferroics and the path to the market, Nat Mater. 18 (2019) 191–192.
[11] J. Ma, J. Hu, Z. Li, C.W. Nan, Recent progress in multiferroic magnetoelectric composites: from bulk to thin films, Adv Mater. 23 (2011) 1062–1087.
[12] S.K. Ghosh, K. Roy, H.K. Mishra, M.R. Sahoo, B. Mahanty, P.N. Vishwakarma, et al., Rollable Magnetoelectric Energy Harvester as a Wireless IoT Sensor, ACS Sustain Chem Eng. 8 (2019) 864–873.
[13] F. Narita, Z. Wang, H. Kurita, Z. Li, Y. Shi, Y. Jia, et al., A Review of Piezoelectric and Magnetostrictive Biosensor Materials for Detection of COVID-19 and Other Viruses, Adv Mater. 33 (2021) e2005448.
[14] F. Spizzo, G. Greco, L. Del Bianco, M. Coïsson, N.M. Pugno, Magnetostrictive and Electroconductive Stress-Sensitive Functional Spider Silk, Adv Funct Mater. 2207382 (2022).
[15] S.P. Kharat, R. Swadipta, R.C. Kambale, Y.D. Kolekar, C.V. Ramana, Enhanced magnetostrictive properties of nanocrystalline Dy^{3+} substituted Fe-rich $Co_{0.8}Fe_{2.2}O_4$ for sensor applications, J Appl Phys. 122 (2017), 164101.
[16] Y.Q. Hu, N.T. Liu, J. Lao, R.H. Liang, X. Deng, Z. Guan, et al., Ultrahigh Ferroelectric and Piezoelectric Properties in $BiFeO_3$-$BaTiO_3$ Epitaxial Films Near Morphotropic Phase Boundary, ACS Appl Mater Interfaces. 14 (2022) 36825–36833.
[17] W. Liu, X. Ren, Large Piezoelectric Effect in Pb-Free Ceramics, Phys Rev Lett. 103 (25) (2009), 257602.
[18] Y. Liu, H. Aziguli, B. Zhang, W. Xu, W. Lu, J. Bernholc, et al., Ferroelectric polymers exhibiting behaviour reminiscent of a morphotropic phase boundary, Nature. 562 (2018) 96–100.
[19] A. Hossain, S. Roy, K. Sakthipandi, The external and internal influences on the tuning of the properties of perovskites: An overview, Ceram Int. 45 (4) (2019) 4152–4166.
[20] Ramana CV, Bandi M, N Nair A, Manciu FS, Sreenivasan S, Shutthanandan V. Electronic Structure, Chemical Bonding, and Electrocatalytic Activity of Ba $(Fe_{0.7}Ta_{0.3})O_{3-\delta}$ Compounds. ACS Appl Energy Mater. 2021; 4 (2): 1313-22.
[21] W. Liu, X. Ren, Large piezoelectric effect in Pb-free ceramics, Physical review letters. 103 (2009), 257602.

[22] E. Ahilandeswari, K. Sakthipandi, R. Rajesh Kanna, M. Hubálovská, D. Vigneswaran, Lanthanum substitution effect on the structural, optical, and dielectrical properties of nanocrystalline $BaFe_2O_4$ ferrites, Physica B Condens. 635 (2022), 413849.

[23] E. Ahilandeswari, R. Rajesh Kanna, K. Sakthipandi, Synthesis of neodymium-doped barium nanoferrite: Analysis of structural, optical, morphological, and magnetic properties, Physica B Condens. 599 (2020), 412425.

[24] C.V. Ramana, Rare-Earth Substituted Magnetostrictive Ferrites: A Case Study of Gadolinium (Gd) Substituted Cobalt Ferrite, in: A.-.-G. Olabi (Ed.), Ency Smart Mater, Elsevier, Oxford, 2022, pp. 134–159.

[25] H.J. Liu, C.K. Wang, D. Su, T. Amrillah, Y.H. Hsieh, K.H. Wu, et al., Flexible Heteroepitaxy of $CoFe_2O_4$/Muscovite Bimorph with Large Magnetostriction, ACS Appl Mater Interfaces. 9 (2017) 7297–7304.

[26] M. Ge, D. Xu, Z. Chen, C. Wei, Y. Zhang, C. Yang, et al., Magnetostrictive-Piezoelectric-Triggered Nanocatalytic Tumor Therapy, Nano Lett. 21 (2021) 6764–6772.

[27] H. Palneedi, V. Annapureddy, S. Priya, J. Ryu, Status and Perspectives of Multiferroic Magnetoelectric Composite Materials and Applications, Actuators. 5 (2016) 9.

[28] Z. Chu, M. PourhosseiniAsl, S. Dong, Review of multi-layered magnetoelectric composite materials and devices applications, J Phys D. 51 (2018), 243001.

[29] J.V. Suchetelene, Product Properties: A New Application of Composite Materials, Philips Res Rep. 27 (1972) 28–37.

[30] A.R. Abraham, B. Raneesh, S. Joseph, P. Mohammed Arif, P.M.G. Nambissan, D. Das, et al., Magnetic performance and defect characterization studies of core-shell architectured $MgFe_2O_4$@$BaTiO_3$ multiferroic nanostructures, Phys Chem Chem Phys. 21 (2019) 8709–8720.

[31] S.K. Upadhyay, V.R. Reddy, S.M. Gupta, N. Chauhan, A. Gupta, Reduced leakage current and improved ferroelectricity in magneto-electric composite ceramics prepared with microwave assisted radiant hybrid sintering, AIP Adv. 5 (2015), 047135.

[32] S.P. Kharat, S.K. Gaikwad, P.G. Nalam, R.C. Kambale, A.R. James, Y.D. Kolekar, et al., Effect of Crystal Structure and Phase on the Dielectric, Ferroelectric, and Piezoelectric Properties of Ca^{2+}- and Zr^{4+}-Substituted Barium Titanate, Cryst Growth Des 22 (2022) 5571–5581.

[33] B.D. Cullity, S.R. Stock, Elements of X-ray Diffraction, Prentice-Hall, New York, 2001.

[34] C.V. Ramana, K.K. Bharathi, A. Garcia, A.L. Campbell, Growth Behavior, Lattice Expansion, Strain, and Surface Morphology of Nanocrystalline, Monoclinic HfO_2 Thin Films, J Phys Chem C. 116 (18) (2012) 9955–9960.

[35] S. Roy, C.V. Ramana, Effect of sintering temperature on the chemical bonding, electronic structure and electrical transport properties of β-$Ga_{1.9}Fe_{0.1}O_3$ compounds, J Mater Sci Technol. 67 (2021) 135–144.

[36] S.M. Ansari, B.B. Sinha, D. Phase, D. Sen, P.U. Sastry, Y.D. Kolekar, et al., Particle Size, Morphology, and Chemical Composition Controlled $CoFe_2O_4$ Nanoparticles with Tunable Magnetic Properties via Oleic Acid Based Solvothermal Synthesis for Application in Electronic Devices, ACS Appl Nano Mater. 2 (4) (2019) 1828–1843.

[37] M.T. Rahman, J. McCloy, C.V. Ramana, R. Panat, Structure, electrical characteristics, and high-temperature stability of aerosol jet printed silver nanoparticle films, J Appl Phys. 120 (7) (2016), 075305.

[38] I.B. Bersuker, V. Polinger, Perovskite Crystals: Unique Pseudo-Jahn–Teller Origin of Ferroelectricity, Multiferroicity, Permittivity, Flexoelectricity, and Polar Nanoregions, Condens Matter. 5 (2020) 68.

[39] X.N. Zhu, W. Zhang, X.M. Chen, Enhanced dielectric and ferroelectric characteristics in Ca-modified $BaTiO_3$ ceramics, AIP Adv. 3 (2013), 082125.

[40] V.S. Puli, S. Adireddy, C.V. Ramana, Chemical bonding and magnetic properties of gadolinium (Gd) substituted cobalt ferrite, J Alloys Compd. 644 (2015) 470–475.

[41] N.R. Kalidindi, F.S. Manciu, C.V. Ramana, Crystal structure, phase, and electrical conductivity of nanocrystalline $W_{0.95}Ti_{0.05}O_3$ thin films, ACS Appl Mater Interfaces. 3 (2011) 863–868.

[42] Z. Lazarevic NR. Characterization of Barium Titanate Ceramic Powders by Raman Spectroscopy. Acta Phys Pol. 2019; 115: 808-10.

[43] F.D. Saccone, S. Ferrari, D. Errandonea, F. Grinblat, V. Bilovol, S. Agouram, Cobalt ferrite nanoparticles under high pressure, J Appl Phys. 118 (2015), 075903.

[44] J.L. Parsons, L. Rimai, Raman spectrum of $BaTiO_3$, Solid State Commun. 5 (1967) 423–427.

[45] Y.-K. Choi, T. Hoshina, H. Takeda, T. Tsurumi, Effect of Oxygen Vacancy and Oxygen Vacancy Migration on Dielectric Response of $BaTiO_3$-Based Ceramics, Jpn J Appl Phys. 50 (2011), 031504.

[46] P.A. Shaikh, R.C. Kambale, A.V. Rao, Y.D. Kolekar, Comparative studies on structural and electrical properties of lead titanate synthesized by ceramic and co-precipitation method, J Alloys Compd. 486 (2009) 442–446.

[47] C.V. Ramana, A. Ait-Salah, S. Utsunomiya, J.-F. Morhange, A. Mauger, F. Gendron, et al., Spectroscopic and Chemical Imaging Analysis of Lithium Iron Triphosphate, J Phys Chem C. 111 (2007) 1049–1054.

[48] C.V. Ramana, A. Ait-Salah, S. Utsunomiya, A. Mauger, F. Gendron, C.M. Julien, Novel Lithium Iron Pyrophosphate ($LiFe_{1.5}P_2O_7$) as a Positive Electrode for Li-Ion Batteries, Chem Mater. 19 (2007) 5319–5324.

[49] M. Etier, C. Schmitz-Antoniak, S. Salamon, H. Trivedi, Y. Gao, A. Nazrabi, et al., Magnetoelectric coupling on multiferroic cobalt ferrite–barium titanate ceramic composites with different connectivity schemes, Acta Mater. 90 (2015) 1–9.

[50] Y. Bakış, I.A. Auwal, B. Ünal, A. Baykal, Maxwell-Wagner relaxation in grain boundary of $BaBi_xLa_xY_xFe_{12-3x}O_{19}$ ($0.0 \leq x \leq 0.33$) hexaferrites, Compos B: Eng. 99 (2016) 248–256.

[51] S.R. Batool, S. Aman, F. Aftab, M.S. Waheed, M.A. Malana, S. Gouadria, et al., Synthesis, Characterization, Dielectric and Magnetic Properties of Substituted Y-Type Hexaferrites, J Mater Sci Mater Electron. 33 (2022) 16183–16196.

[52] H. Huo, X. Li, Y. Chen, J. Liang, S. Deng, X. Gao, et al., Bifunctional composite separator with a solid-state-battery strategy for dendrite-free lithium metal batteries, Energy Stor Mater. 29 (2020) 361–366.

[53] D. Damjanovic, M. Demartin, Contribution of the irreversible displacement of domain walls to the piezoelectric effect in barium titanate and lead zirconate titanate ceramics, J Phys Condens Matter. 9 (1997) 4943–4953.

[54] W. Xia, J. Zhou, T. Hu, P. Ren, G. Zhu, Y. Yin, et al., Enhanced magnetoelectric coefficient and interfacial compatibility by constructing a three-phase CFO@BT@PDA/P(VDF-TrFE) core-shell nanocomposite, Compos A: Appl Sci Manuf. 131 (2020), 105805.

[55] W. Xia, J. Zhou, T. Hu, P. Ren, G. Zhu, Y. Yin, et al., Enhanced magnetoelectric coefficient and interfacial compatibility by constructing a three-phase CFO@BT@PDA/P(VDF-TrFE) core-shell nanocomposite, Appl Sci Manuf, Compos A, 2020, p. 131.

[56] M. Rasly, M. Afifi, A.E. Shalan, M.M. Rashad, A quantitative model based on an experimental study for the magnetoelectric coupling at the interface of cobalt ferrite–barium titanate nanocomposites, Appl Phys A 123 (5) (2017) 331.

[57] E.V. Ramana, F. Figueiras, M.P. Graca, M.A. Valente, Observation of magnetoelectric coupling and local piezoresponse in modified $(Na_{0.5}Bi_{0.5})TiO_3$-$BaTiO_3$-$CoFe_2O_4$ lead-free composites, Dalton Trans. 43 (26) (2014) 9934–9943.

[58] S.N. Babu, K. Srinivas, T. Bhimasankaram, Studies on lead-free multiferroic magnetoelectric composites, J Magn Magn Mater. 321 (22) (2009) 3764–3770.

[59] F. Safi Samghabadi, L. Chang, M. Khodadadi, K.S. Martirosyan, D. Litvinov, Scalable, cost-efficient synthesis and properties optimization of magnetoelectric cobalt ferrite/barium titanate composites, APL Mater. 9 (2) (2021), 021104.

[60] W. Santa-Rosa, P.S. da Silva, J.-C. M'Peko, H. Amorín, M. Algueró, M. Venet, Enhanced piezomagnetic coefficient of cobalt ferrite ceramics by Ga and Mn doping for magnetoelectric applications, J Appl Phys. 125 (7) (2019), 075107.

[61] A. Baji, Y.-W. Mai, R. Yimnirun, S. Unruan, Electrospun barium titanate/cobalt ferrite composite fibers with improved magnetoelectric performance, RSC Adv. 4 (98) (2014) 55217–55223.

[62] C.T. De Leo, G.C. Dannangoda, M.A. Hobosyan, J.T. Held, F.S. Samghabadi, M. Khodadadi, et al., Carbon combustion synthesis of Janus-like particles of magnetoelectric cobalt ferrite and barium titanate, Ceram Int. 47 (4) (2021) 5415–5422.

[63] D.M. Ghone, S. Premkumar, K.K. Patankar, S.D. Kaushik, V.L. Mathe, Enhanced strain derivative of Ho substituted cobalt ferrite and improved magnetoelectric coupling in co-sintered bi-layered ME composites, Sens Actuator A Phys. 301 (2020), 111716.

[64] M.E. Botello-Zubiate, D. Bueno-BaquÉS, J.D.F. Vaquerizo, L.E. Fuentes Cobas, J. A. Matutes-Aquino, Synthesis and Magnetoelectric Characterization of Cobalt Ferrite—Barium Titanate Composites Using a New Pulsed Magnetic Field Method, Integr Ferroelectr. 83 (1) (2006) 33–40.